

Crack propagation in polystyrene under fixed elongation

KALYAN SEHANOBISH, ERIC BAER, ALEXANDER CHUDNOVSKY,
ABDELSAMIE MOET

*Department of Macromolecular Science, Case Western Reserve University, Cleveland,
Ohio 44106, USA*

Microscopic observations of precracked polystyrene samples under fixed elongation conditions reveal that discontinuous crack propagation occurs under stress relaxation asymptotically approaching a stable configuration. A zone of intensive crazes in the vicinity of the crack tip evolves concurrently with crack growth. The evolution of the crazed zone occurs as translation and isotropic expansion. The phenomenon has been successfully explained using a crack layer model. Crack propagation is found to be controlled by the difference between the energy dissipated on damage (crazing) growth and the relevant energy release rate.

1. Introduction

Studies of the stress relaxation of polymers under relatively large strains are usually directed towards characterizing relaxation moduli and thus the load-bearing capability of the material. Recently, such studies are also used to identify the criteria for the onset of irreversible deformation events [1-4] and to examine environmental effects [5-7]. Although fracture was observed under stress relaxation conditions, particularly in the presence of active environments, no attempts to model fracture propagation kinetics in polymers are known to the authors.

Realizing that crack initiation followed by slow crack propagation are the two major components in the lifetime of an engineering structure, efforts were directed to establish laws of crack propagation. It is believed that initially existing defects may act as crack starters, thus determination of crack growth kinetics should suffice to make reasonable lifetime predictions. On this premise, intensive modelling of fatigue crack propagation has been advanced. Minimal efforts, however, were directed to developing laws for creep crack propagation. Even fewer are the attempts to study crack propagation under stress relaxation conditions. Formalisms of creep crack kinetics follow the stream of fatigue crack models most of which rest on the original idea of Griffith [8] that fracture

propagates as an ideal cut. For example, Gent and Hirakawa [9] described creep crack growth in styrene-modified rubber as

$$\frac{dc}{dt} = 3 \times 10^{-5} \left(\frac{S}{S_0} \right)^3 \quad (1)$$

where S and S_0 are Griffith's surface energy at any time t and minimum value of surface energy for the crack growth to occur. The front factor and the exponent used in Equation 1 were believed to be material constants. Since then several investigators have promoted the use of the stress intensity factor K to describe creep crack growth in polymers. Relationships of the general form

$$\frac{dc}{dt} = f(K) \quad (2)$$

were suggested [10-13]. Attempts to discover a general law of creep fracture, apart from the actual failure mechanisms, lead to unique constitutive equations for each of the polymers studied under specific loading conditions.

Studying fracture kinetics in precracked structures under fixed displacement is certainly of practical importance. Crack propagation under diminishing stress indeed raises interesting questions regarding the mechanism of fracture and its cause. This paper reports the results of an experiment designed to examine fracture propagation

behaviour of polystyrene under stress relaxation. The kinetics of the phenomenon is explained in terms of a quantitative account of the concurrently observed mechanisms.

2. Experimental procedure

The material used in this investigation was a plane isotropic extruded sheet (0.25 mm thick) of polystyrene obtained from Transilwrap Corporation (Cleveland, Ohio). The draw ratio of the material was approximately 1.8 in the two mutually perpendicular directions. Standard tensile tests showed that the Young modulus (E) was $\cong 2.2$ GPa, the tensile fracture stress was $\cong 60$ MPa, and the ultimate elongation over 60 mm gauge length was $\cong 3.5\%$.

A straight notch of 4 mm depth was introduced into rectangular specimens of 20 mm \times 80 mm at a rate of 0.5 mm min^{-1} using a razor blade fitted to the crosshead of an Instron machine. The edges were then carefully polished using metallographic techniques to 0.3 μm final finish. Polished samples were annealed in a vacuum oven at 90°C for 48 h and allowed to cool slowly (10°C h^{-1}) to room temperature.

The tensile behaviour of single edge notched (SEN) specimens is shown in Fig. 1. The sample was monotonically loaded past the point B (Fig. 1) at a strain rate of 1.0% min^{-1} and then held under fixed elongation. Crack growth and craze evolution were simultaneously observed using a motor driven 35 mm camera attached to a Nikon optical microscope. The microscope-camera assembly was mounted on a movable stage fitted with a micrometer, thus providing crack length measurements with precision of a hundredth of a milli-

metre. Stress-relaxation occurs in the sample for ~ 20 h eventually reaching an equilibrium value. Photographs of the crack and the surrounding crazed zone were taken at various stages of relaxation and analysed.

After 100 h the specimen was unloaded, then broken under monotonic loading at a strain rate of 1.0% min^{-1} . The fracture surface of the specimen was studied under optical and scanning electron microscopes.

3. Results

Three separate experiments were performed on identical SEN specimens. Although the exact values of the initial conditions (stress and strain) varied from specimen to specimen, the crack propagation mechanisms and the stress-relaxation behaviour of all three specimens displayed a good reproducibility. The quantitative analysis provided in this report has been based on one experiment.

A semilogarithmic composite plot of the crack growth kinetics and stress-relaxation behaviour is shown in Fig. 2. The initial dotted and solid lines indicate crack growth and the corresponding stress rise during the monotonic loading of the specimen. During this period of monotonic loading the remote stress (at the grips) rose to 26.3 MPa and the crack grew about 0.31 mm. The specimen was then held under fixed grips at this stress level. Crack growth continued for the next 2 h accompanied by stress-relaxation. Significant discontinuities in the rate of relaxation and crack growth were observed during this period. The rate of relaxation first decreased and then increased, while the crack growth rate continued to decrease. At the end of the first 2 h the crack growth was

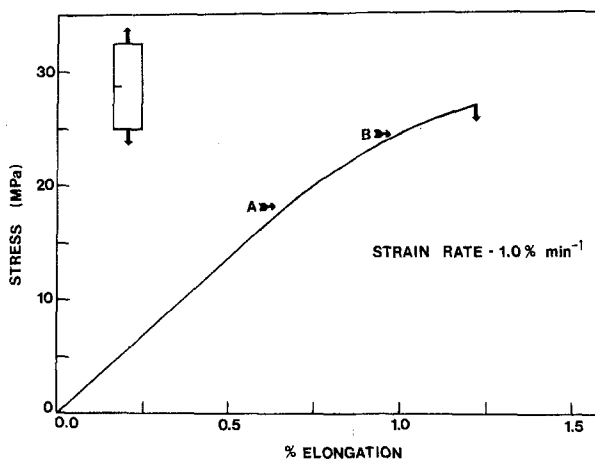


Figure 1 Stress-elongation diagram of SEN polystyrene samples. Arrows A and B point to craze initiation and crack initiation, respectively.

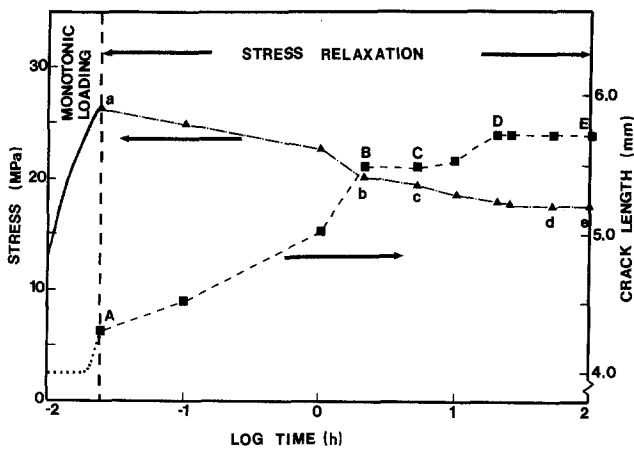


Figure 2 Composite plot of stress-relaxation behaviour and crack growth kinetics in precracked PS. The crack grows discontinuously under decreasing stress.

abruptly arrested (BC in Fig. 2) for the next 3 h, while the stress-relaxation continued to occur (bc). The crack resumed its growth afterwards to be arrested again at point D after which no more crack propagation was observed for the next 80 h until the experiment was terminated. Although the crack ceased to propagate, an appreciable reduction in the remote stress was noticed until point d (Fig. 2), beyond which no significant relaxation could be measured. Finer details of this discontinuous crack growth were clearly revealed from the fractographic analysis as will be demonstrated later. Fig. 3 illustrates how the crack growth rate decayed until the final crack arrest.

An optical micrograph exhibiting a typical side view of the crack and the associated crazed zone is shown in Fig. 4. Contrary to the dominantly accepted image of an ideal cut, the crack propagated preceded by a layer of an intense crazed zone displaying a "candle flame" pattern. Concurrent with the stress-relaxation, the crazed zone

translated and expanded. A halo of diffuse surface crazes (region H in Fig. 4) slowly began to appear surrounding the leading front of the intense crazed zone. The "halo" crazes spread over the entire specimen with time. Crack propagation, however, occurred through the most intense part of the candle flame crazed zone.

A more lucid view of the interaction between craze growth and crack propagation is illustrated in Fig. 5. The figure exhibits the evolution of the crack and the crazed zone as directly traced from optical micrographs similar to Fig. 4 but magnified 1.5 times. Points A to F (Fig. 5) indicate the locations of the crack tip at various stages of relaxation. During the initial stages of relaxation, the advancement of the crack tip is always accompanied by advancement of the crazed zone tip (points A₁, B₁, C₁) until the crack is arrested at C. This crack arrest corresponds to the first visible

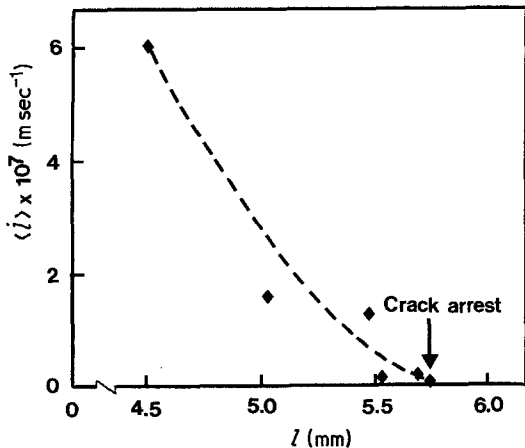


Figure 3 Crack growth rate \dot{l} against crack length.

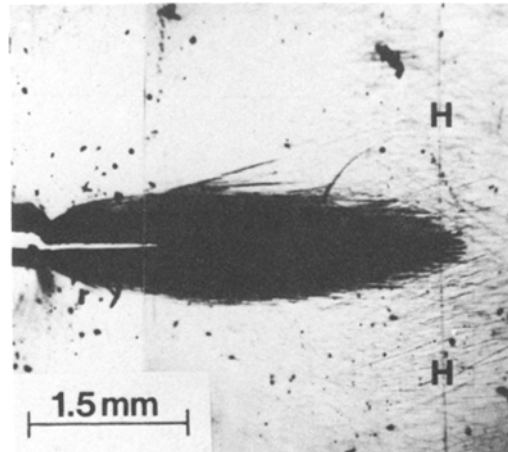


Figure 4 Optical micrograph displaying the evolution of "through" crazes surrounding the crack tip. Zone H consists of diffuse surface crazes.

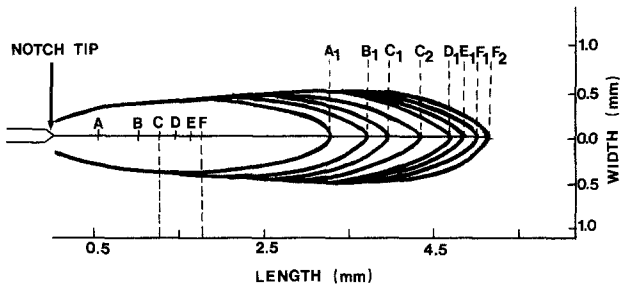


Figure 5 Composite plot showing crack growth and evolution of the crazed zone. Vertical markers (A through F) indicate crack tip positions.

crack arrest indicated in Fig. 2 (BC). Although the crack remains arrested at C for 3 h the crazed zone propagates from C_1 to C_2 . During this period the material undergoes considerable relaxation as indicated in Fig. 2. Once more the crack resumes its growth to be arrested again at location F (Fig. 5). Similar to the first crack arrest at C, the candle flame crazed zone continues its propagation with time from F_1 to F_2 . This craze growth also results in considerable stress-relaxation although at a decaying rate.

A more detailed understanding of the crack-crazed zone propagation can be gained by considering the geometric evolution of the crazed zone. As shown in Figs. 4 and 5, the crazed zone appears to be approximately elliptical in shape and can be characterized by its major and minor axes. Fig. 6 indicates that $l_a(t)$ and $w(t)$ normalized with respect to the final values l_a and w , i.e. $l_a(t)/l_a$ and $w(t)/w$, respectively, increase with crack length in a monotonic fashion. The ratio of crazed zone length to width remains nearly constant during the entire history studied. This indicates that the crazed zone expands in a self-similar

manner irrespective of the discontinuous crack growth.

After 100 h the specimen was unloaded and then reloaded to fracture at a strain rate of $1.0\% \text{ min}^{-1}$. The relationship of the remote stress (load divided by the initial cross-sectional area) to the overall elongation is shown in Fig. 7. It is interesting to note that the stress-strain behaviour now shows an initial "toe region" where the change in stress with respect to strain, $d\sigma/d\varepsilon$, steadily increases. Through a smooth transition, the toe region is followed by a linear region of constant effective modulus (1.65 GPa) prior to fracture. Note that this effective modulus is considerably lower than the elastic modulus of the notched sample prior to crack-craze propagation (2.1 GPa). This behaviour clearly reflects the microstructure of the crazed zone and the associated crack growth.

Micrographs of the fracture surface taken from the region of slow crack propagation are shown in Fig. 8. It is well recognized that fracture surface striations are caused by a discontinuous crack advance. This discontinuous crack growth pattern is well documented here by the striated morphology of the fracture surface (Fig. 8a). It should be noted here that it is usually believed that striations are typical of fatigue loading caused by alternate cycles of loading and unloading. The first striation indicated by arrow A on the fractograph (Fig. 8a) corresponds to the crack length measured after 6 min (Fig. 2). Arrow \nearrow just prior to the first striation marks the position of the crack tip (point A in Fig. 2) upon disrupting the movement of the crosshead. The absence of striation corresponding to this location indicates that crack growth was not immediately interrupted upon stopping the movement of the crosshead. Although only two complete crack arrests were observed from kinetic measurements (Fig. 2), detailed microscopic study of the fracture surface shows the presence of seven distinct striations. Striations indicated by arrows A, C, D,

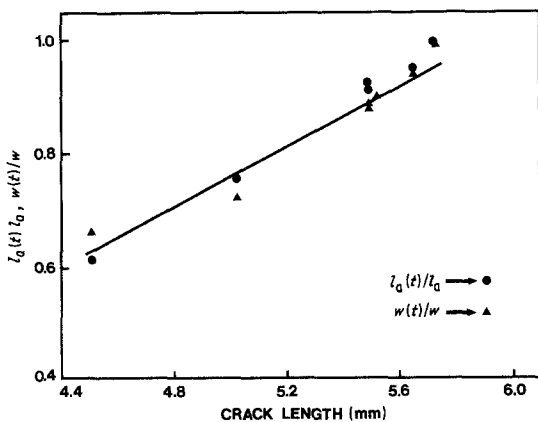


Figure 6 Plots of the ratio of instantaneous active zone length ($l_a(t)$) to final length (l_a) and the ratio of instantaneous active zone width ($w(t)$) to the final width (w) against crack length.

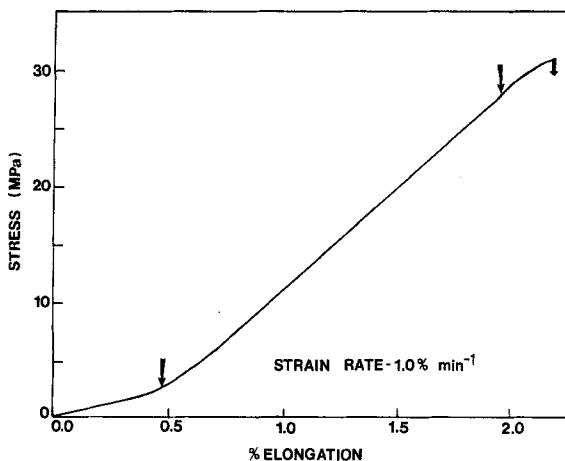


Figure 7 Stress-elongation behaviour of the relaxed specimen after unloading.

E and F are obviously caused by short-duration crack arrests. Instead of appearing as clear steps (e.g. B to C in Fig. 2) they appear as discontinuities in crack growth rate (between points A to B in Fig. 2). No more striations were noticed beyond 1.7 mm from the notch tip. This agrees fairly well with the ultimate crack arrest between points D to E of Fig. 2.

At a distance of 2.1 mm from the striation G, a curved striation H associated with a sharp morpho-

logical change is observed. This curved striation usually corresponds to the transition from slow crack growth to avalanche-like (uncontrolled) crack propagation. This transition involves large-scale tearing of drawn material (arrow T in Fig. 8b). Elliptical fissures grown perpendicular to the fracture surface are observed within the transition region (Fig. 8c). The critical crack length corresponding to uncontrolled crack propagation has been identified (arrow C in Fig. 15a)

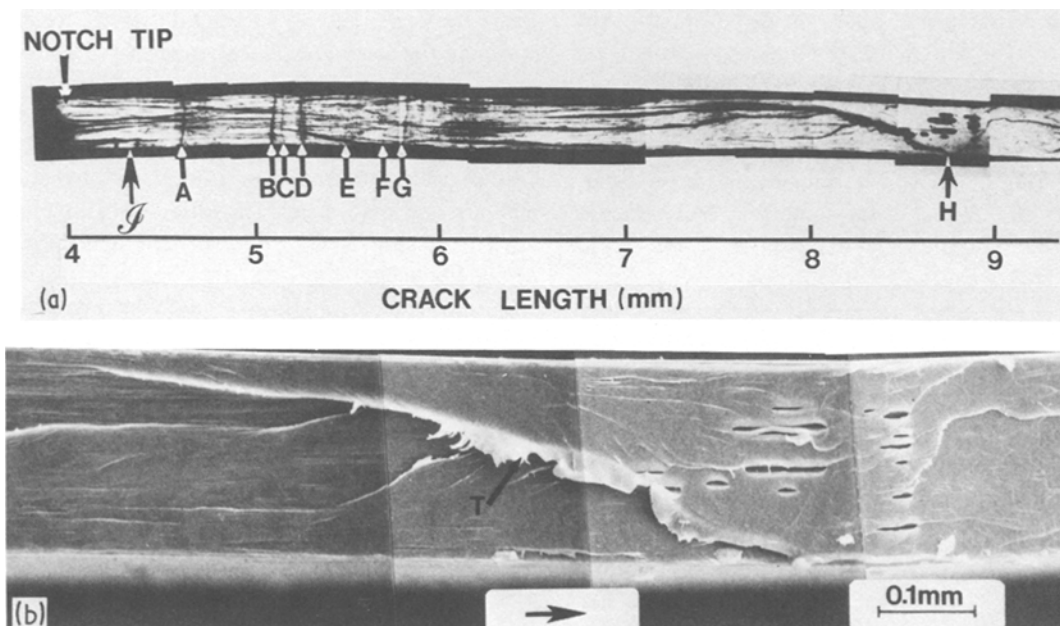


Figure 8 (a) Optical micrograph of the fracture surface displaying discontinuous crack growth bands A through G during stress-relaxation of 100 h. Arrow H indicates the location where the curved striation terminates signalling uncontrolled crack propagation during subsequent monotonic load. (b) Scanning electron micrograph of the fracture surface showing large-scale tearing (arrow T) of the drawn material associated with the striation H in Fig. 8a. The horizontal arrow indicates the crack propagation. (c) Scanning electron micrographs of the fracture surface showing elliptical fissures grown perpendicular to the fracture surface.

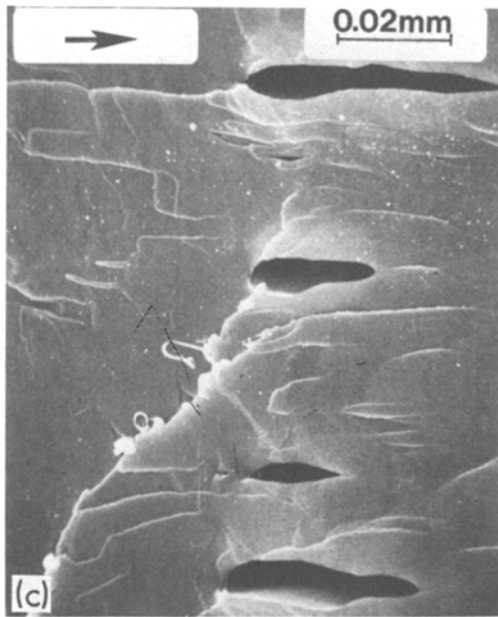


Figure 8 Continued.

by correlating the side view with the fracture surface.

4. Discussion

The results described above reveal the nature of fracture propagation under stress relaxation conditions and raise several questions, most of which are addressed in this section.

1. It is commonly accepted that the crack propagation rate can be presented as a function of the stress intensity factor K . In comparison with others, the function $G = K^2/E$ has a clear physical meaning as the elastic energy release rate. For our experiment G can be calculated as

$$G = \frac{\sigma^2 \pi l}{E} f^2 \left(\frac{l}{B} \right) \quad (3)$$

Here, σ is the remote stress, E is Young's modulus, l is the crack length and B is the width of the specimen. The correction factor $f(l/B)$ accounting for the specimen geometry has been evaluated according to the elastic solution of the boundary value problem [14], i.e.

$$f\left(\frac{l}{B}\right) = 1.12 - 0.231 \left(\frac{l}{B}\right) + 10.55 \left(\frac{l}{B}\right)^2 - 21.72 \left(\frac{l}{B}\right)^3 + 30.39 \left(\frac{l}{B}\right)^4 \quad (4)$$

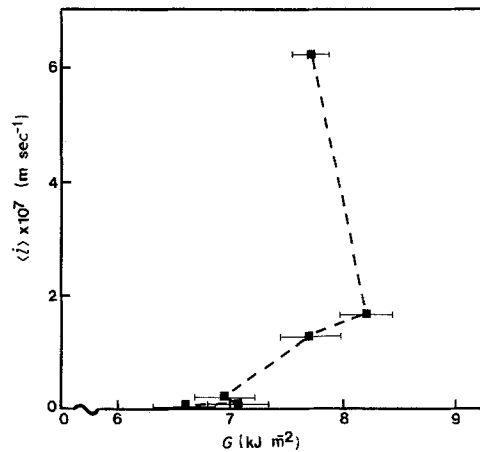


Figure 9 Crack growth rate \dot{l} against energy release rate G .

The average crack growth rate as a function of G is shown in Fig. 9. The curve indicates the absence of a unique relationship between \dot{l} and G . Clearly \dot{l} cannot appropriately correlate with G . Thus linear elastic fracture mechanics (LEFM) is inadequate for the present case. The demonstrated inadequacy stems from the fact that LEFM concepts are based on the idea that fracture advances as an ideal cut, perceived by Griffith [8]. However, it is quite evident from the observed results that the crack does not propagate as an ideal cut.

2. In view of the fact that the crack is preceded and surrounded by a large crazed zone, plastic zone models are examined. The simplest is the line plastic zone model proposed by Dugdale [15] and Barenblatt [16]. This model has gained wide, yet controversial, applicability to polymers [17–22]. The Dugdale–Barenblatt model relates the plastic zone size r to the energy release rate as

$$r = \frac{\pi GE}{8\sigma_y^2} \quad (5)$$

Several authors [23–25] have also correlated the band width b on the fracture surface to the plastic zone size. The Dugdale–Barenblatt plastic zone size r , the observed craze zone size l_a and the fracture band width b are presented in relation to the energy release rate G in Fig. 10. Both the craze zone size l_a and fracture band width b do not display a linear relationship with G . Hence, ductile fracture mechanics based on the idea of a line plastic zone may not be applicable to our case.

3. It may be argued that the craze zone preceding the crack may be treated as the plastic zone proposed by nonlinear fracture mechanics [26].

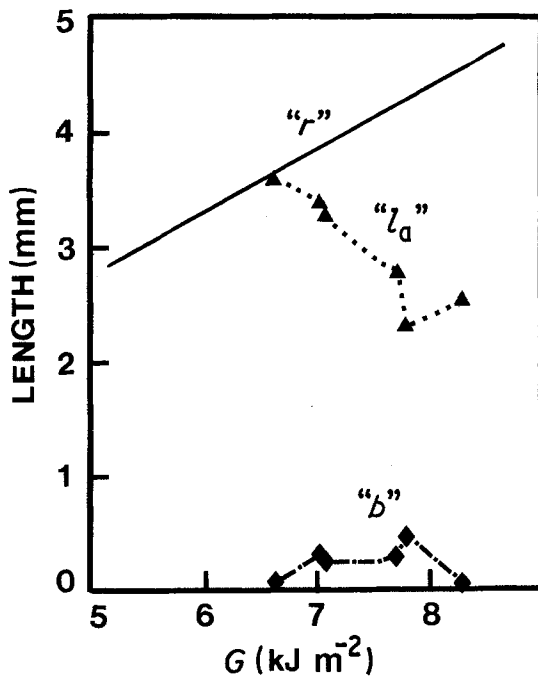


Figure 10 Relationship of fracture band widths b and active zone length l_a to the energy release rate G compared with the predicted plastic zone size r (solid line).

Now, we examine this proposition from three different angles. First, the side view of the craze zone (Fig. 4) is different from that predicted by the theory of plasticity for plane stress or plane strain conditions [27]. Secondly, a cross-section taken perpendicular to the crack propagation plane, in the vicinity of the crack tip (Fig. 11a) shows that the craze zone profile is qualitatively different from that predicted from the theory of plasticity. The cross-sectional profile of the plastic zone (Fig. 11b) is created due to dominant plane stress conditions near the traction-free surface and plane strain state at the centre [27]. However, the craze zone profile in our case does not show the slightest resemblance to the plastic zone profile. Thirdly, the plastic zone size obtained from elastoplastic fracture mechanics is uniquely related to the crack length, yet craze zone growth is found to occur at constant crack length (Fig. 5). Two different craze zone sizes indicated by markers C_1 and C_2 are observed at the same crack length indicated by C . The same is again repeated at the location marked F .

One can foresee a modification of conventional plasticity to describe the observed side view of the crazed zone thus eliminating the first discrepancy. However, the second and particularly the third

discrepancies are clear indications of the inapplicability of conventional plasticity.

4. A system of a crack and the surrounding damage is considered as a crack layer (CL). The active zone is part of the CL within which the rate of damage growth is positive [28–31]. CL propagation appears as active zone movements: translation; rotation; deformation; isotropic expansion and shape changes. The driving forces corresponding to these elements of movement are identified within the framework of irreversible thermodynamics. A thermodynamic force is usually introduced whose product with the corresponding flux gives entropy production due to the processes considered.

Considering the observed geometric evolution of the active zone (Fig. 6) we may conclude that CL propagation involves only translation and expansion of the active zone. A closer look at Fig. 5 confirms this fact. The active zone continues to expand even when the crack remains arrested. Thus, active zone expansion (e) appears as an independent degree of freedom. The entropy production associated with the CL propagation (translation and expansion) can be expressed in the following bilinear form [28–31]:

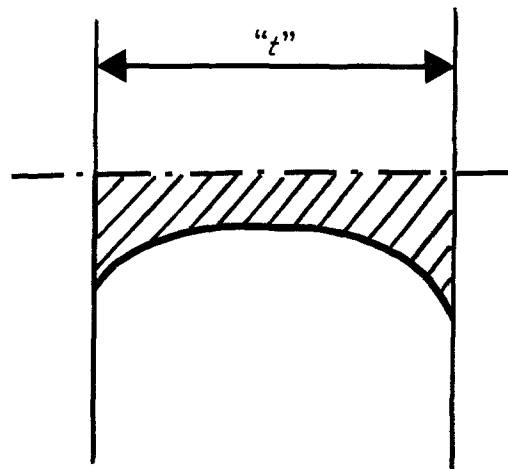
$$T\dot{S}_i = \dot{D} + \dot{X}^{(t)} + \dot{e}X^{(e)} \quad (6)$$

Here, the rates of CL extension \dot{l} and expansion \dot{e} are the thermodynamic fluxes. The conjugate thermodynamic forces are $X^{(t)}$ and $X^{(e)}$, respectively. D is the energy dissipated in craze formation and growth, a part of which ($\beta_1 D$) is expended in CL translation and the rest expended on expansion. In order to explain the decay in the crack growth rate and the final crack arrest displayed in Fig. 3, only the translational mode of propagation needs to be considered.

The translational driving force has been identified as $J_1 - \gamma^* R_1$, where J_1 is the energy release rate, γ^* is the specific enthalpy of damage (crazing in the present case), and R_1 is the translational resistance moment. The latter can be evaluated as $R_1 = \langle \rho \rangle w$, where $\langle \rho \rangle$ is the average crazing density [29]. Applying the principle of minimal entropy production, which yields $\dot{S}_i = 0$ for this case, we obtain the law of translational CL propagation as [30, 31]

$$\dot{l} = \frac{\beta_1 \dot{D}}{\gamma^* R_1 - J_1} \quad (7)$$

whereas $\gamma^* R_1$ expresses the energy required for CL



(b)

Figure 11 (a) Transverse section taken perpendicular to crack propagation plane illustrates the craze zone profile. (b) Cross-sectional profile predicted from elastoplastic solution.

mines the nature of crack propagation. Below we briefly explain the procedure by which $\gamma^*R_1 - J_1$ is evaluated.

4.1. Evaluation of energy barrier

1. The energy required γ^*R_1 is proportional to the width w of the active zone. The coefficient of proportionality $\gamma^*\langle\rho\rangle$ is taken from a related analysis [32]. The evolution of w is taken from Fig. 6.

2. The energy release rate J_1 is conventionally expressed in terms of the elastic stress and displacement fields outside the damage zone [33, 34]. In the above discussion we established the inapplicability of plasticity to model the observed crazed zone. Thus, one cannot make use of the elastoplastic solution available in the literature. A recently developed semiempirical technique for energy release rate calculation [35–37] has been employed.

The energy release rate J_1 is the negative first partial derivative of the elastic potential energy of the solid due to the translation of a crack headed by an active zone, i.e.

$$J_1 = -\frac{\partial P}{\partial l} \quad (8)$$

For our case, under fixed elongation condition, P is given by

$$P = F_\epsilon = \frac{1}{2} \mathcal{F} \Delta \quad (9)$$

where, F_ϵ is the strain energy, \mathcal{F} and Δ are the

translation, J_1 expresses the energy *available* for the process. Thus the denominator ($\gamma^*R_1 - J_1$) is but the energy barrier to crack propagation. It is the evolution of the energy barrier which deter-

load and displacement at the grip respectively. Hence from Equations 8 and 9

$$J_1 = -\frac{1}{2} \left[\Delta \frac{d\mathcal{F}}{dl} + \mathcal{F} \frac{d\Delta}{dl} \right] \quad (10)$$

For fixed elongation condition

$$\frac{d\Delta}{dl} = 0 \quad (11)$$

consequently,

$$J_1 = -\frac{1}{2} \Delta \frac{d\mathcal{F}}{dl} \quad (12)$$

where $d\mathcal{F}$ is the drop in load at the grips caused by translation of the crack and the crazed zone. $d\mathcal{F}$ has been evaluated using a recently developed stress analysis technique illustrated elsewhere [35]. This technique evaluates displacement at the grips due to growth of the crazed zone using a second Green tensor of elasticity. Finally, the displacements are converted into forces on the basis of a superposition principle applicable to a linear elastic medium. Since, the total displacement Δ at the grip is known and dl is available from crack length measurements, J_1 can be evaluated.

The energy release rate J_1 so calculated, together with G , for comparison are plotted as a function of the crack length l (Fig. 12). Notably, both G and J_1 tend to decrease with increase in crack length.

Evolution of the energy barrier as a function of crack length is demonstrated by the shadowed zone between γ^*R_1 and J_1 in Fig. 13. Clearly, the energy barrier increases as the crack advances.

4.2. Evaluation of energy dissipation rate

The rate of energy dissipation on craze formation and growth, \dot{D} is defined as

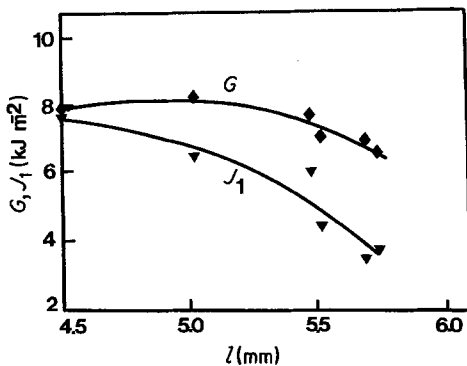


Figure 12 Composite plot of energy release rate G and semiempirically calculated J_1 against crack length.

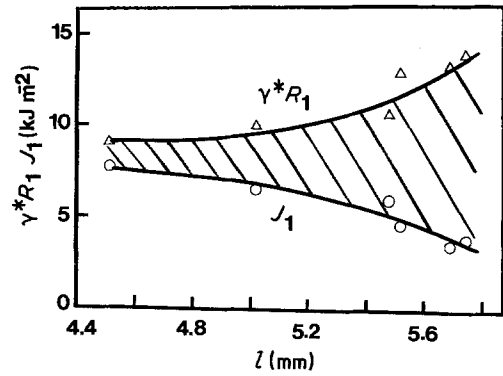


Figure 13 Energy required for crack propagation γ^*R_1 and energy released J_1 plotted against crack length l . The shadowed area demonstrates evolution of the energy barrier $\gamma^*R_1 - J_1$.

$$\dot{D} = \dot{W}_i - \dot{Q} \quad (13)$$

where W_i is the work done on irreversible deformation and Q is the part of this work converted into heat. In the present situation, the amount of heat generated Q was not measured, thus we assume \dot{D} to be proportional to \dot{W}_i . The rate of irreversible work \dot{W}_i done by the applied load \mathcal{F} at the grips on the displacement at the grips Δ_{cr} due to the growth of the craze zone is

$$\dot{W}_i = \mathcal{F} \cdot \dot{\Delta}_{cr} \quad (14)$$

As mentioned earlier, Δ_{cr} can be evaluated using a second Green tensor of elasticity. The rate of irreversible work \dot{W}_i evaluated using Equation 14 is plotted as a function of crack length (Fig. 14). Thus, \dot{D} ($\sim \dot{W}_i$) vanishes as the stress-relaxation process is halted. The cooperative effect of the increase of the energy barrier ($\gamma^*R_1 - J_1$) and the decrease of the dissipation rate $\beta_1 \dot{D}$ explains in terms of Equation 7 the observed decay in the crack growth rate \dot{l} as well as the final crack arrest ($\dot{l} = 0$).

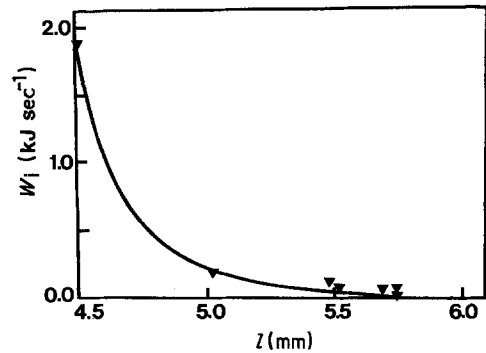


Figure 14 Rate of irreversible work \dot{W}_i against crack length l .

Knowledge of the fracture stress and the critical crack length yields critical energy release rates of 11.6 kJ m^{-2} for unrelaxed specimens (Fig. 15b) and 36.3 kJ m^{-2} for relaxed specimens (Fig. 15a). This result is explained by the CL theory. Indeed, according to the CL theory, the critical value of J_1 , i.e. J_{1c} is proportional to the resistant moment R_{1c} [32]:

$$J_{1c} = \gamma^* R_{1c} = \gamma w_c \quad (15)$$

The critical width of the active zone w_c for the relaxed specimen (at arrow C in Fig. 15a) is estimated as three times that of the initial specimen at the notch tip, Fig. 15b. Thus, the threefold increase in fracture toughness is directly related to a similar increase in the extent of crazing. This result is in good agreement with the recently reported loading history dependency of the critical energy release rate [32, 38].

5. Conclusions

1. Discontinuous crack propagation occurs under stress-relaxation loading even below the monotonic crack initiation stress.

2. The crack is preceded by a dense crazed zone. Fracture advances as interactive leaps of the crazed zone and the crack.

3. The experimental results are successfully explained on the basis of the crack layer theory. The cooperative effect of the increase of energy barrier ($\gamma^* R_1 - J_1$) and decrease of the dissipation rate $\beta_1 D$ explains the decay in crack growth rate as well as the final crack arrest.

4. As predicted by the crack layer theory, the presence of the crazed zone ahead of the crack is found to increase the critical energy release rate (fracture toughness) markedly.

Acknowledgement

The authors gratefully acknowledge the financial support of the Office of Naval Research (ONR) through grant number N000-14-75-C-0795.

References

1. E. J. KRAMER and R. A. BUBECK, *J. Polym. Sci. Polym. Phys. Ed.* **16** (1978) 1195.
2. O. S. BRULLER, *Polymer* **19** (1978) 1195.
3. A. S. ARGON and M. M. SALAMA, *Phil. Mag.* **36** (1977) 1217.
4. J. B. C. WU and N. BROWN, *J. Rheol.* **23** (1979) 231.
5. A. MOET, I. PALLEY and E. BAER, *J. Appl. Phys.* **51** (1980) 10.
6. L. H. TUNG, *J. Polym. Sci. A3* (1965) 1845.
7. E. GAUBE, *Kunststoffe* **49** (1959) 446.
8. A. A. GRIFFITH, *Phil Trans. Soc. (London)* **A221** (1920) 163.
9. A. N. GENT and H. HIRAKAWA, *J. Polym. Sci. A6* (1968) 1481.
10. G. P. MARSHALL, L. E. CULVER and J. G. WILLIAMS, *Plast. Polym.* **37** (1969) 75.
11. W. G. KNAUSS, *Int. J. Fract. Mech.* **6** (1970) 7.
12. M. KITAGAWA and K. MOTOMURA, *J. Polym. Sci. Polym. Phys. Ed.* **12** (1974) 1979.
13. S. R. PRICE and D. HULL, *J. Mater. Sci.* **18** (1983) 2795.
14. H. TADA, P. C. PARIS and G. P. IRWIN, "The Stress Analysis of Cracks Handbook" (Del Research Corporation, Helertown, Pa. 1973).
15. D. S. DUGDALE, *J. Mech. Phys. Sol.* **8** (1960) 100.
16. D. I. BARENBLATT, *Adv. Appl. Mech.* **7** (1962) 55.
17. H. R. BROWN and I. M. WARD, *Polymer* **14** (1973) 469.
18. M. J. DOYLE and J. G. WAGNER, in Proceedings of the ACS Symposium on Toughness and Brittleness of Plastics, September 1976, edited by R. D. Deanin and A. D. Crugnola, in chemistry series 154 (ACS), p. 63.
19. W. DÖLL and G. W. WEIDMANN, *Prog. Colloid. Polym. Sci.* **66** (1979) 291.

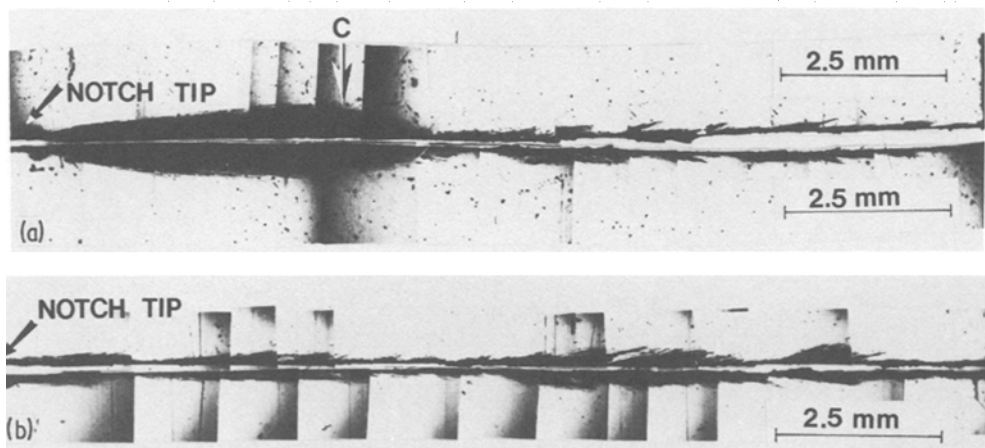


Figure 15 Side view of the fracture surface corresponding to the stress-elongation diagram of (a) Fig. 7, (b) Fig. 1.

20. S. J. ISRAEL, E. L. THOMAS and W. W. GERBERICH, *J. Mater. Sci.* **14** (1979) 2128.
21. W. WANG and E. J. KRAMER, *ibid.* **17** (1982) 2013.
22. W. DÖLL, U. SHIEDELMANN and L. KÖNCZÖL, *ibid.* **15** (1980) 2389.
23. R. W. HERTZBERG, *Int. J. Fract.* **15** (1979) R69.
24. J. P. E. LINK, J. C. BAUMENS and G. HOWES, *Int. J. Fract. Mech.* **7** (1971) 277.
25. R. SCHIRRER, R. LANG, J. MANSON and B. TOMATIS, *Polym. Eng. Sci.* **24** (1984) 820.
26. J. W. HUTCHINSON, "Nonlinear Fracture Mechanics" (Technical University of Denmark, 1979).
27. D. BROEK, "Elementary Engineering Fracture Mechanics" (Martinus Nijhoff Publishers, The Hague, 1982).
28. V. A. KHANDOGIN and A. CHUDNOVSKY, "Dynamika Prochnost Aviacionnyh Konstrukcy" (Novosibirsk, USSR, 1978).
29. A. CHUDNOVSKY, NASA report, in press.
30. A. MOET and A. CHUDNOVSKY, *Polym. Eng. Sci.* **22** (1982) 84.
31. A. CHUDNOVSKY and A. MOET, Sixth International Conference on Fracture, New Delhi, India, 1984, submitted.
32. N. HADDAOUI, A. CHUDNOVSKY and A. MOET, *Polym. Mater. Eng. Sci.* **49** (1983) 117.
33. J. R. RICE, *J. Appl. Mech.* **35** (1968) 379.
34. G. P. CHEREPANOV, *J. Appl. Math. Mech.* [translation] **31** (1967) 304.
35. A. DOLGOPOLSKY, PhD thesis, Case Western Reserve University, Cleveland, Ohio (1983).
36. K. SEHANOBISH, A. MOET and A. CHUDNOVSKY, to be published.
37. J. BOTSIS, A. MOET and A. CHUDNOVSKY, to be published.
38. M. BAKAR, A. MOET and A. CHUDNOVSKY, International Conference of Fatigue in Polymers, The Rubber and Plastic Institute, London, June, 1983, paper no. 8.

*Received 25 January
and accepted 21 June 1984*